Journal of Radioanalytical and Nuclear Chemistry (2020) 323:51–59
https://doi.org/10.1007/s10967-019-06955-2

Ag_2WO_4 nanoparticles radiolabeled with technetium-99m: a potential new tool for tumor identification and uptake

Carla Júnia Santos[1] · Francisco Moura Filho[1] · Fernanda Lapa Campos[2] · Carolina de Aguiar Ferreira[3] · André Luís Branco de Barros[2] · Daniel Crístian Ferreira Soares[1]

Received: 12 March 2019 / Published online: 26 November 2019

Abstract
Silver tungstate nanoparticles have been presenting attractive characteristics that could allow its usage in the biomedical sciences. In this study, Ag_2WO_4 nanoparticles with an average size of 242 nm were obtained and radiolabeled with technetium-99m with high labeling-yield as well as high stability. Biodistribution studies were carried out in healthy and tumor-bearing mice to determine the nanoparticle's in vivo behavior. The results revealed an important tumor-to-muscle ratio, reaching values above than 1.5, demonstrated the ability of this nanomaterial in accumulating preferentially in tumor tissue. All results together, converge to consider the Ag_2WO_4 nanoparticles as a potential system against cancer and a potential new radiolabeled probe for tumor identification and uptake.

Keywords [^{99m}Tc]–Ag_2WO_4 nanoparticles · Ag_2WO_4 tumor probe · Ag_2WO_4 tumor-bearing mice biodistribution

Introduction

The use of silver and silver ions in medicine is nothing new: their applicability dates back to the Neolithic revolution and owing to its bactericidal properties, their medicinal use is reported since the eighth century. Silver nitrate aqueous solutions were used for the topical treatment of infections throughout the nineteenth century [1, 2]. From that time onwards, the use of silver has extrapolated that sole purpose and several other silver compounds have been developed for and employed in different areas, such as material science, engineering, and biomedicine.

Among silver compounds, silver tungstate, a monovalent tungstate with the minimum formula Ag_2WO_4, has attracted considerable attention in recent years due to their physical and chemical properties that enable a wide range of applications. Silver tungstate (herein mentioned as α-Ag_2WO_4) is a ceramic material that presents structural polymorphism with three different crystalline phases in which the α phase, is the thermodynamically more stable [3–6].

α-Ag_2WO_4 nanomaterials have been extensively recognized for their photoluminescence and ability to degrade organic pollutants under UV light irradiation [5, 7–13]. Besides, α-Ag_2WO_4 nanoparticles have also been applied as gas sensors with good sensitivity even at low ozone and acetone concentrations [14, 15]. Moreover, interesting biological properties have been demonstrated for this type of metal oxide and it has been used as antimicrobial and anticancer agents [16–19]. Since this type of nanoparticle has shown promising results for biological applications, especially in the cancer therapy and diagnosis field, it is essential to have a deep understanding of their in vivo behavior [20–22]. However, to date, no studies on the biodistribution profile of this material, either in healthy or tumor-bearing animals have been carried out. In this context, herein, we have synthesized and characterized Ag_2WO_4 nanoparticles and radiolabeled with technetium-99m. The in vivo fate of the radiolabeled nanoparticles in healthy and tumor-bearing mice was evaluated aiming to study the potential use

✉ Daniel Crístian Ferreira Soares
soares@unifei.edu.br

[1] Laboratório de Bioengenharia, Universidade Federal de Itajubá, Rua Irmã Ivone Drumond, 200, Distrito Industrial II, Itabira, Minas Gerais 35903-087, Brazil

[2] Faculdade de Farmácia, Universidade Federal de Minas Gerais, Avenida Presidente Antônio Carlos 6627, Pampulha, Belo Horizonte, Minas Gerais 31270-901, Brazil

[3] Department of Biomedical Engineering, University of Wisconsin-Madison, Highland Avenue, 1111, Madison, WI 53705, USA

of [^{99m}Tc]α–Ag_2WO_4 nanoparticles as a new tool for tumor identification and uptake.

Experimental

Materials

Sodium tungstate dihydrate (purity > 99%), was purchased from Specsol (São Paulo, Brazil) and silver nitrate (purity > 99.8%) was obtained from Alphatec (São Paulo, Brazil). Stannous chloride was purchased from Sigma-Aldrich (São Paulo, Brazil). Sodium chloride (NaCl) was obtained from Merck (Rio de Janeiro, Brazil). Sigma-Aldrich (São Paulo, Brazil). Technetium-99m was obtained from an alumina-based ^{99}Mo/^{99m}Tc generator. Water was purified using a Milli-Q apparatus (Millipore, Billerica, USA). All other chemicals and reagents used in this study were of analytical grade. Ehrlich cell line was purchased from American Type Culture Collection (ATCC® CCL-77™, Manassas, USA). Trypan blue dye was purchased from Sigma-Aldrich (São Paulo, Brazil). Whatman™ 3MM chromatography paper was acquired from Sigma-Aldrich (São Paulo, Brazil). Female Swiss mice (6–8-week-old) were obtained from CEBIO-UFMG (Belo Horizonte, Brazil).

Ag_2WO_4 nanoparticles synthesis

Silver tungstate (α-Ag_2WO_4) nanoparticles were prepared through microwave-assisted hydrothermal synthesis (MAHS) following a previously described method by LONGO and co-workers with some modifications [15]. Briefly, 1.0×10^{-3} mol of tungstate sodium dihydrate and 2.0×10^{-3} mol of silver nitrate were separately dissolved in 20 mL deionized water and heated to 80 °C for 10 min, with constant stirring. The resultant solutions were then mixed and, the obtained suspension was added to a Teflon container and then exposed to microwave oven operating at a frequency of 2.45 GHz (800 W) at 130 °C for 60 min (heating rate of 15 °C min^{-1}). After cooling, the obtained precipitate was centrifuged 5 × (32,000×*g*—5 min) and resuspended with 40 mL deionized water (5x) and 40 mL of acetone (1x). The resultant solid was classified (< 400 nm) through 0.4 µm filter. Finally, the obtained material was dried at 70 °C for 4 h.

Physicochemical characterization

X-ray diffractometry

The identification of the main phase present in the nanoparticles was conducted through X-ray Diffraction (XRD) technique, using a Rigaku wide-angle SmartLab equipped with a vertical goniometer. The analysis was made applying CuKα radiation (λ = 1.54060 nm) measured in step scan mode with steps of 0.02°2′ θ and a scan speed of 1.00° s^{-1} from 10 to 80°2′ θ. The crystallite size was calculated from the simple and well-known Scherrer equation. The main peak was used for the procedure, take into account the value of 0.9 radians for the constant β [23].

Raman spectroscopy

Raman spectra were performed on Micro Raman spectrometer (HORIBA IHR 320) with a 320 nm wavelength coupled with a microscope (OLYMPUS BX-41). To obtain the Raman spectra, the samples were placed on a polished glass surface on the stage of a microscope. The Raman spectra were excited by a solid-state laser producing highly polarized light at 633 nm and collected at a resolution of 2 cm^{-1} and a precision of ± 1 cm^{-1} in the range between 50 and 1000 cm^{-1}. Repeated acquisitions, using the highest magnification (50×), were carried out to improve the signal-to-noise ratio in the spectra. Spectra were calibrated using the 520.5 cm^{-1} line of a silicon wafer.

Mean size, polydispersity index and zeta potential analyses

The average hydrodynamic size (AHS), size distribution and zeta potential (ζ) were determined using dynamic light scattering (DLS) and phase analysis light scattering (PALS) in a Zetasizer Nano–ZS equipped with 40 mW, 633 nm laser (Model ZEN 360, Malvern Instruments Ltd, Malvern, UK). The mean size and polydispersity index of the α-Ag_2WO_4 were evaluated by DLS, at 25 °C, and an angle of 90°. The zeta potential was determined by DLS associated with electrophoretic mobility, at pH 7.4, and an angle of 90°. All analyses were performed in a Nano ZS Zetasizer (Malvern Instruments Ltd, Worcestershire, UK). Triplicates of dispersion at 1 µg mL^{-1} of α-Ag_2WO_4 were prepared with ultra-pure water (120 ± 20 µS cm^{-2} of conductivity). The mean size, polydispersity index, and zeta potential data were obtained after to vigorous shaking in a vortex.

Radiolabeling and radiochemical purity evaluation

The radiolabeling procedures were carried out as previously described by Monteiro et al. [24], with a few modifications. Briefly, an aliquot of 100 µL of the α-Ag_2WO_4 (2 mg mL^{-1}) was added to 200 µL of acidic $SnCl_2$ aqueous solution (1 mg mL^{-1}). Then, the pH was adjusted to 7.0, the vial was sealed, and the air was removed with a syringe. Afterward, 100 µL of sodium pertechnetate ([^{99m}Tc]$NaTcO_4$) (37 MBq) in 0.9% (w/v) NaCl was added and the mixture was kept at room temperature for 15 min. The labeling vial was rinse with 500 µL of saline (0.9% w/v NaCl) and the content was

transferred to an Eppendorf tube and then centrifuged at 10,000×*g* for 10 min for sample purification. The supernatant was then removed, and the pellet was resuspended with 500 µL of saline using an ultrasonic bath.

Radiochemical yield was evaluated through thin layer chromatography (TLC) method using Whatman™ chromatography paper (Whatman™ 3MM, GE Whatman, Maidstone, United Kingdom) before and after purification by centrifugation. Methylethylketone was used as mobile phase to quantify the free [^{99m}Tc]TcO_4^- ($R_f = 0.9$; whereas [^{99m}Tc]TcO_2 and [^{99m}Tc]α–Ag_2WO_4 show $R_f = 0.0$–0.2). The radioactivity was quantified by a gamma counter (Wallac Wizard 1470–020 Gamma Counter; PerkinElmer Inc., Waltham, Massachusetts, USA). The obtained solution was purified from [^{99m}Tc]TcO_2 during the centrifugation step described above, and the radiochemical yield was calculated through the difference in the radioactivity according to the equation:

$$\% \text{ labeling} = (\text{pellet}/(\text{pellet} + \text{supernatant})) \times 100 \quad (1)$$

In vitro radiolabeling stability evaluation

In vitro studies were performed to evaluate the radiolabeling stability of [^{99m}Tc]α–Ag_2WO_4. The procedure was previously conducted according to studies of Oda et al., [25]. The radiolabeling stability was tested in NaCl 0.9% (w/v) at room temperature and in mouse plasma (100 µL of [^{99m}Tc]α–Ag_2WO_4—10 µg, 3.7 MBq in 1 mL of fresh mouse plasma) at 37 °C, both under agitation. Aliquots of 5 µL were taken out at 1, 2, 4 and 24 h, and analyzed by TLC. Additionally, the AHS of radiolabeled Ag_2WO_4 nanoparticles was determined using DLS technique.

Blood clearance evaluation

100 µL of [^{99m}Tc]α–Ag_2WO_4 (10 µg, 3.7 MBq) was injected to healthy Swiss female mice ($n = 7$) through tail vein injection, and blood samples (10 µL) were collected at 1, 5, 10, 15, 30, 45, 60, 90, 120, 240, 480 and 1440 min post-administration. Then, each sample was weighed, and the associated radioactivity was determined in an automatic scintillation apparatus (Wallac Wizard 1470–020 Gamma Counter; PerkinElmer Inc., Waltham, Massachusetts, USA). The percentage injected dose per gram (%ID g^{-1}) and its mean ± SD were determined, and the data is plotted as a function of time.

In vitro tumor model

The procedure was based on previous studies conducted by Soares et al., [26]. Ehrlich ascites carcinoma cells (1.0×10^6 cells) were intraperitoneally injected into the abdominal cavity of Swiss female mice. Ascites fluid was collected on the 10th day after tumor cells injection. The Ehrlich cells were washed twice and then resuspended in 5 mL of saline solution (0.9% w/v NaCl). An aliquot of the cell suspension was stained with trypan blue (1:1) and counted in Neubauer chamber to determine cell viability. An aliquot of 100 µL, containing 1×10^7 cells, were then injected subcutaneously into the right thigh of Swiss female mice (6–8 weeks, $n = 14$). The mice were kept in groups of seven animals per cage, with free access to food and water under a light–dark cycle of 12 h (beginning at 06:30 a.m.) and controlled temperature (24 ± 1 °C) for 8 days until the tumor reached a mean tumor volume of 103 ± 17 mm^3. Ehrlich tumor-bearing mice were used for biodistribution studies. All animal studies were approved by the local Ethics Committee for Animal Experiments (CEUA/UFMG) under the protocol number 376/2016.

Biodistribution studies

Healthy and Ehrlich tumor-bearing Swiss female mice were used in the biodistribution studies. To each animal, an aliquot of 3.7 MBq of [^{99m}Tc]α–Ag_2WO_4 (10 µg, $n = 7$) was injected intravenously. After 1 h and 4 h, mice were anesthetized with a mixture of xylazine (15 mg kg^{-1}) and ketamine (80 mg kg^{-1}) and euthanized by cervical dislocation. Liver, spleen, kidney, stomach, heart, lungs, thyroid, intestines, brain and muscle were removed, dried on filter paper, and placed in pre-weighed plastic test tubes. The radioactivity was measured using an automatic gamma counter. A standard dosage containing the same injected amount was counted simultaneously in a separate tube, which was defined as 100% radioactivity. The results are expressed as the percentage of injected dose/g of tissue (%ID/g).

Statistical analysis

The characterization data were analyzed employing Origin Pro 8.5 (OriginLab Corporation, Massachusetts, USA). Student *t* test was applied in the biodistribution studies and, the tumor accumulation ratio evaluation. One-way ANOVA and Tukey post hoc test were used in the in vitro stability study of [^{99m}Tc]α–Ag2WO_4 employing the GraphPad Prism® 5.0 Software. Data were expressed as mean ± standard deviation (SD). Statistical significance was accepted when $p < 0.05$.

Results and discussion

α-Ag_2WO_4 nanoparticles were synthesized through the microwave-assisted hydrothermal synthesis (MAHS) approach, following a two-step method. In the first step, sodium tungstate and silver nitrate salts were separately

dissolved in ultra-pure water in which the ionization reactions (2) and (3) occurred. The aqueous solution containing the Ag^+ ions was added to the WO_4^- aqueous solution using a magnetic stirring for mixing. A pale-yellow suspension was instantaneously obtained (Fig. 1) and a white precipitate could be promptly observed as the solid product described in the reaction (4).

$$2AgNO_{3(s)} \rightarrow 2Ag^{+}_{(aq)} + 2NO^{-}_{3(aq)} \quad (2)$$

$$Na_2WO_{4(s)} \cdot 2H_2O_{(s)} \rightarrow 2Na^{+}_{(aq)} + WO^{2-}_{4(aq)} + 2H_2O_{(l)} \quad (3)$$

$$2Ag^{+}_{(aq)} + WO^{2-}_{4(aq)} \rightarrow \alpha\text{-}Ag_2WO_{4(s)} \quad (4)$$

In the second step, the obtained precipitate was hydrothermally treated in a microwave oven at 130 °C for 60 min The resulting suspension presented a gray appearance, which was maintained even after the complete material drying.

Since the pioneering work of Gedye et al. [29] and Giguere et al. [30] the MAHS approach has been established as a good alternative method for synthesis, especially for allowing the possibility of obtaining particles with high purity and crystallinity, in the nanoscale, in a much less time consuming process [13, 27–30]. Da Silva and co-workers [15] synthesized α-Ag_2WO_4 nanorods through MAHS approach and reported important properties of the obtained material for applications such as the gas detection in biological samples and potential non-invasive diagnosis of diabetes. Analysis of gaseous metabolites has been used, over the past years, as a useful tool for the noninvasive diagnosis and monitoring of a broad range of diseases [31, 32]. Acetone, for example, has been used as a specific marker for the diabetes diagnosis and efforts have been made towards the discovery of novel acetone-sensing devices.

Recent studies have demonstrated interesting biological properties for α-Ag_2WO_4 nanoparticles. Longo and co-workers [16], i.e., have demonstrated potent antibacterial activity for this material against methicillin-resistant *S. aureus*. Considering the cancer research field, Muthamizh and co-workers [33] revealed a dose-dependent decrease in the viability of mice melanoma cells treated with silver tungstate nanoparticles. Besides, the biocompatibility of this nanoparticles was tested on normal skin cell line (human keratinocyte), with promising results. Silver tungstate exhibited no significant cytotoxicity effect against human keratinocyte cell line [19]. However, studies involving the toxicity effects of these nanoparticles are scarce and more investigations need to be conducted to evaluate adequately the potential risks.

Fig. 1 Ag_2WO_4 nanoparticles suspension obtained by MAHS method

Physicochemical characterization

Xrd

The structural ordering at long range of the α-Ag_2WO_4 crystals was evaluated by XRD patterns analysis and the results are available in Fig. 2. The intense and well-defined peaks can be correlated to the orthorhombic phase, non-centrosymmetric space group Pn2n, point-group of

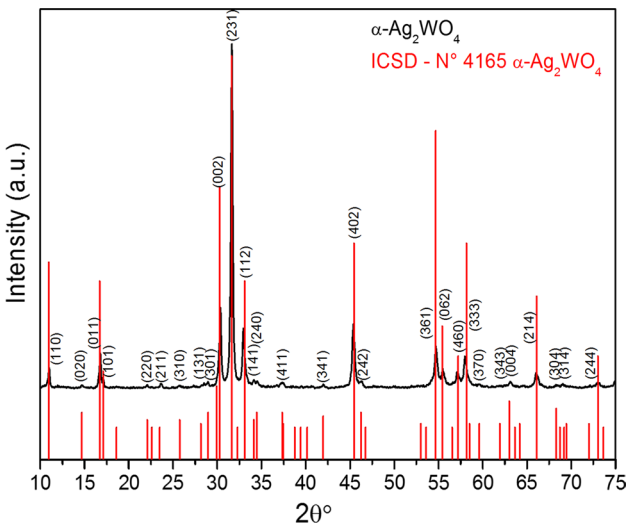

Fig. 2 XRD patterns of α-Ag_2WO_4 nanoparticles prepared through MAHS at 130 °C. The vertical lines (|) indicate the positions and intensities found in ICSD card no. 4165, which corresponds to the α-Ag_2WO_4 phase

symmetry C10/2v and two molecular formulas per unit cell ($Z=2$) of α-Ag_2WO_4. All the diffraction peaks are in accordance with the Inorganic Crystal Structure Database (ICSD) no. 4165 pattern and indicates the phase purity of the samples.

Scherrer's equation was used to calculate the average crystallite size of α-Ag_2WO_4 samples. The results revealed an average crystallite size of 47.7 ± 5.56 nm. This result is following recent works published by Pinatti et al. [34] and He et al. [35], where they synthesized Ag_2WO_4 nanorods through co-precipitation method. In these works, the authors calculated the crystallite size around 32 nm and 38 nm, respectively.

Raman spectroscopy

Raman spectroscopy is an excellent technique that allows the observation of structural defects and the crystalline organization of the nanomaterial at short and medium-range. A previous study conducted by Turkovič et al. [36] revealed twenty-one vibrational modes for this material in which was correlated to an orthorhombic structure ($6A_{1g}$, $5A_{2g}$, $5B_{1g}$, and $5B_{2g}$). In this study, 11 vibrational modes were identified, and the results are available in Fig. 3. The weak bands in the range of 200–800 cm^{-1} was attributed to the stretching mode of the [WO_4] cluster, whereas the intense peak at 874 cm^{-1} was attributed to the bending modes of the Ag–O–W. It is possible to observe in the range of 50–100 cm^{-1}, similar band to those reported by Basiev and co-workers [37], which was attributed to movements of the silver cation, relative to the anionic molecular cluster $[WO_4]^{2-}$ (external vibrational modes).

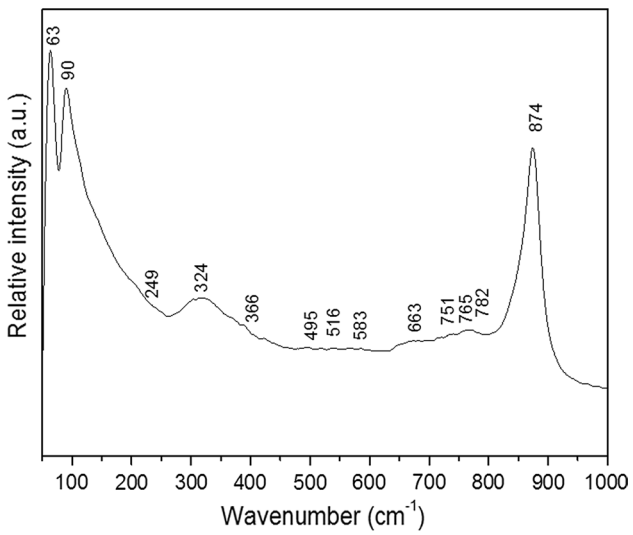

Fig. 3 Raman spectra of the hydrothermally synthesized α-Ag_2WO_4 nanoparticles

Mean size, polydispersity index and zeta potential analysis

According to the photon correlation spectroscopy technique, α-Ag_2WO_4 nanoparticles presented an average hydrodynamic diameter of 242.40 ± 11.89 nm. Furthermore, the syntheses procedures allowed obtaining a monodisperse colloidal system with a significantly negative charge (Table 1).

It is well known that nanoparticles have different pharmacokinetic behavior and biodistribution profile when compared to small molecules, leading to potentially different therapeutic and toxicity characteristics. Importantly, not only its biodistribution but also the interaction between the nanoparticle and the target cells can be affected by its composition and physicochemical properties such as size, shape and zeta potential [38]. Zeta potential, the net charge on a surface of a particle, is a major influential physical factor impacting pharmacokinetics and biodistribution of nanoparticles and is known to affect the nanoparticles internalization at different cells lines [39].

Radiochemical purity and stability

α-Ag_2WO_4 nanoparticles were successfully labeled with ^{99m}Tc with a radiochemical yield of 94.98 ± 2.38%. Radiochemical impurities [^{99m}Tc]TcO_4^- and [^{99m}Tc]TcO_2) were quantified as 1.39 ± 0.65% and 3.68 ± 1.83%, respectively. [^{99m}Tc]TcO_2 was further eliminated by the centrifugation process leading to a radiochemical purity higher than 95% (98.34 ± 1.06%). The radiolabeled nanoparticles exhibited a high in vitro stability (Fig. 4) within 24 h of incubation ($n=5$) in saline and mouse plasma. The AHS of radiolabeled Ag_2WO_4 nanoparticles was determined before and after of incubation process and no significant differences were found in the obtained results, revealing important stability of nanoparticles during the incubation time.

Radiochemical purity higher than 90%, achieved for all tested timepoints in which no statistically significant differences were observed among tested groups. These results are important for in vivo studies, such as biodistribution and scintigraphic images since a non-stable compound can release the radioisotope in the bloodstream allowing to obtain false results regarding the in vivo complex behavior. Furthermore, the presence of radiochemical impurities can result in poor quality images due to high background

Table 1 Polydispersity index and Zeta potential of α-Ag_2WO_4 nanoparticles. The analyses were carried out in ultra-pure water at a concentration of 0.9 mg mL^{-1}, in pH 7.4. All measurements were performed in triplicates at 25 °C

Samples	Polydispersity index	ζ potential (mV)
α-Ag_2WO_4	0.191 ± 0.02	− 26.25 ± 7.28

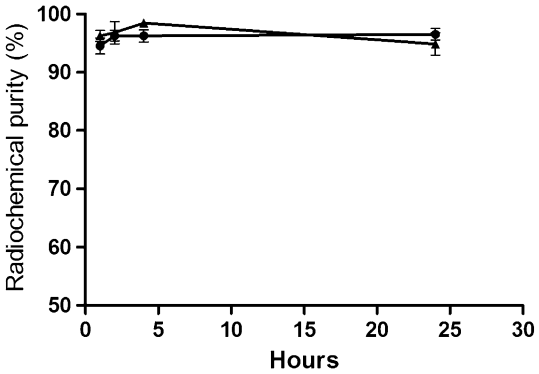

Fig. 4 In vitro stability of [^{99m}Tc]α–Ag_2WO_4 in 0.9% saline solution (circles) at room temperature (25 °C) and in mouse plasma (triangles) at 37 °C. Data expressed as mean ± SD of the mean ($n = 5$)

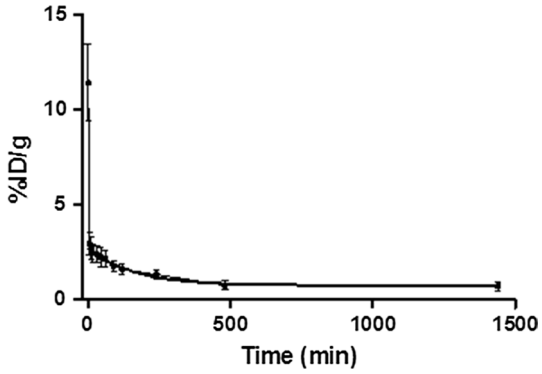

Fig. 5 Clearance profile of [^{99m}Tc]α–Ag_2WO_4 obtained from healthy mice injected i.v. route. The data are expressed as mean percentage of injected dose ± SD of the mean ($n = 7$)

radiation around the tissues and the blood and exposes the patient to an unnecessary dose of radiation [40].

The direct radiolabeling of nanosystems with ^{99m}Tc has been applied to various types of nanoparticles [41–43]. Still in 2004, Fu and co-workers successfully conducted the direct radiolabeling of ferrite nanoparticles with technetium-99m [44]. Wang et al. [45] conducted a more detailed study where ferrite nanoparticles were direct radiolabeled with [^{99m}Tc]$NaTcO_4$, with radiochemical purity over than 92%. According to the authors, technetium atoms can be covalently bonded with the Fe_3O_4 nanoparticles since they have hydroxyl groups in which can easily conjugate with technetium-99m atoms. Otherwise, technetium atoms can conjugate to nanoparticles by Van Der Waals forces, in which low stability can be observed [45]. In this sense, based on the same described mechanism and the radiolabeling stability obtained, we hypothesized a similar behavior for Ag_2WO_4 nanoparticles, where ^{99m}Tc atoms were covalently bonded to the oxygen atoms of crystalline structure. However, additional studies must be conducted to elucidate, in details, the main mechanism involved in this radiolabeling reaction.

Blood clearance and biodistribution studies

In Fig. 5 is available the blood clearance profile obtained from healthy Swiss female mice after intravenous (i.v.) administration of [^{99m}Tc]α–Ag_2WO_4. Blood levels declined following biphasic pattern with an α half-life of 0.83 min and a β half-life of 111.6 min.

In this study, the biodistribution investigations were conducted aiming to assess the location of the [^{99m}Tc]α–Ag_2WO_4 nanoparticles. The biodistribution profile at 1 and 4 h after i.v. injection of the radiolabeled nanosystem into healthy and tumor-bearing mice (Erhlich carcinoma) are available in Figs. 6 and 7, respectively. An important uptake in kidney, liver, and spleen was detected in all studied times that can be attributed to regular physiological routes of elimination. On the other hand, only discrete uptake in the stomach or thyroid was observed, which are regular sites of accumulation of the radiolabeling impurities, such as [^{99m}Tc]TcO_4^- [24]. Based on this fact we can hypothesized that low amounts of [^{99m}Tc]TcO_4^- are present. These results are in agreement with the results obtained in the radiochemical purity test. As expected, biodistribution studies on healthy and tumor-bearing mice showed high uptake in liver and spleen in all tested animals. Such uptake and retention might be attributed to the actions of phagocytic cells belonging to the Mononuclear Phagocyte System (MPS) abundantly present in these organs. In this sense, the uptake observed in the lungs could be attributed to this same reason [25].

In this work, the tumor accumulation behavior can be related to Enhanced Permeability and Retention Effect (EPR effect), where the nanoparticle system can be significantly retained in tumor region due to fenestrations raging 7–400 nm, observed in blood vessels of tumor region [46, 47]. This effect was firstly described by Maeda and Matsumura in 1986 and despite over past 33 years, some questions remain unsolved such as: How phenotype and size of the tumor can influence the EPR effect? How the extension tissue perfusion, necrosis grade, vascularity can alter the drug/nanoparticle uptake? [47, 48]. However, today is well-defined that the EPR effect is controlled by diverse chemical mediators such as cyclooxygenase, tumor necrosis factor-α, vascular epidermal growth factor, matrix metalloproteinase, bradykinin, and etc. For Ehrlich tumor-bearing mice, the tumor-to-muscle ratios obtained from the biodistribution data were calculated for 1 and 4 h and the results revealed ratios of 1.21 after 1 h and 2.74, after 4 h (Fig. 8).

Particularly, in these animals, although the tumor uptake was lower than organs such as liver, spleen, kidneys, and lungs, the values for tumor tissue was consistently higher than those observed for muscle in the same

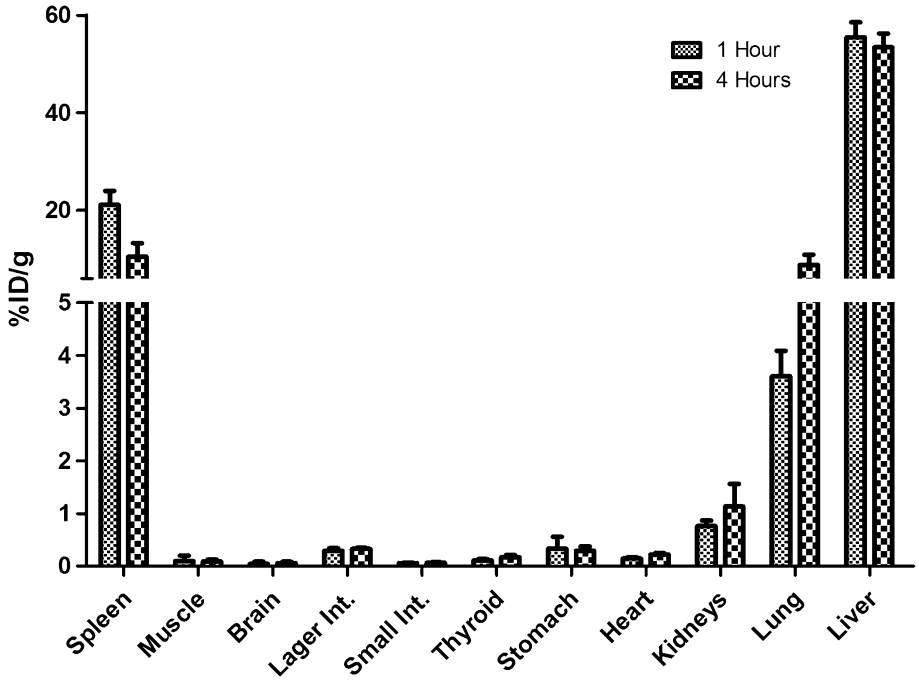

Fig. 6 Biodistribution profile obtained at 1 and 4 h after i.v. administration of [^{99m}Tc]α–Ag_2WO_4 in healthy mice. The data are expressed as the average percentage of the injected dose of [^{99m}Tc]α–Ag_2WO_4 per gram of tissue ± SD of the mean ($n = 7$)

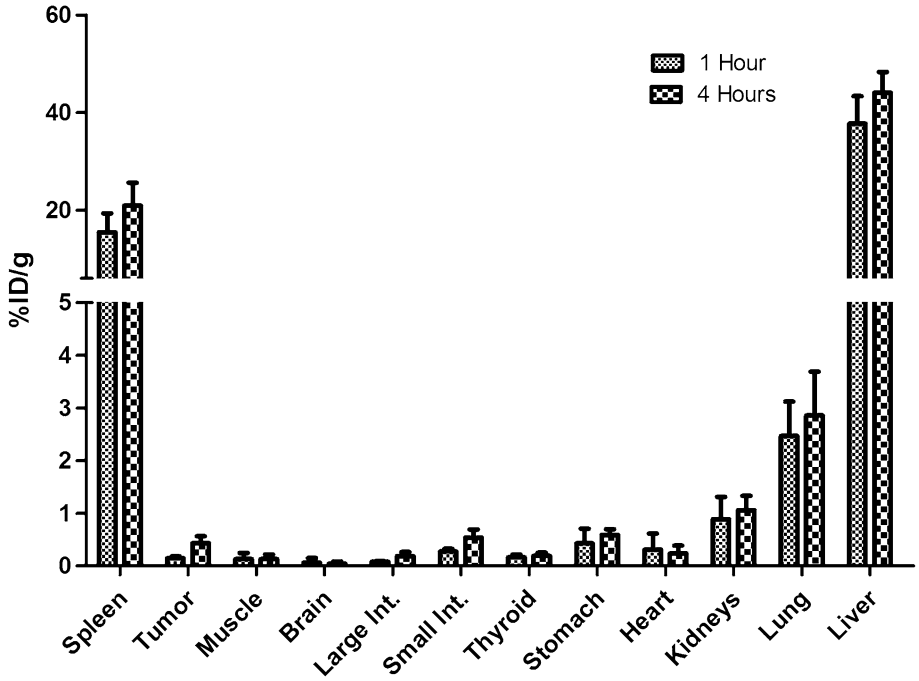

Fig. 7 Biodistribution profile obtained at 1 and 4 h after i.v. administration of [^{99m}Tc]α–Ag_2WO_4 in Ehrlich tumor-bearing mice. The data are expressed as the average percentage of the injected dose of radiolabeled nanoparticles per gram of tissue ± SD of the mean ($n = 7$)

animal (considered as surround control tissue). However, more detailed studies can reveal the detailed mechanism involved in this preferential tumor accumulation as well as to amplify the knowledge of the use of inorganic nanocarriers as radiolabeled probes.

Conclusions

In this study, α-Ag_2WO_4 nanoparticles were successfully obtained through microwave-assisted hydrothermal

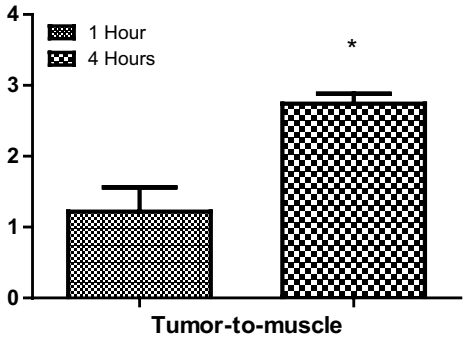

Fig. 8 Tumor-to-Muscle Ratios obtained at 1 and 4 h after i.v. administration of [^{99m}Tc]α–Ag_2WO_4. The data are expressed as average percentage of injected dose of radiolabeled nanoparticles per gram of tissue ± SD of the mean ($n = 7$). Asterisks indicate statistically significant differences between 1 and 4 h ($p < 0.05$) analyzed through non-parametric Student t-test (two-tailed; unpaired test in which unequal variance was assumed)

synthesis. The Raman spectroscopy and X-ray diffractometry data revealed compounds with an important structural organization in the long- and short-range order. The analysis of the polydispersity index and zeta potential suggests that silver tungstate forms a monodisperse and stable suspension in an aqueous medium. Furthermore, the nanoparticles were successfully labeled with technetium-99m with a high radiolabeling yield and biodistribution studies indicated that, although silver tungstate also accumulates on phagocytic cells, the nanoparticles preferentially accumulated in tumor tissue rather than in normal tissues, possibly due to EPR effect. Thus, [^{99m}Tc]α–Ag_2WO_4 can be considered a potential new tool for tumor identification and uptake aiming either cancer diagnostic or therapeutic approaches. Nonetheless, since biological properties of α-Ag_2WO_4 nanoparticles are still poorly explored in the literature, future detailed in vitro and in vivo studies to assess detailed biocompatibility of these nanoparticles are warranted.

Acknowledgements The authors would like to thank Coordenação de Aperfeiçoamento de Pessoal de Nível Superior (CAPES), Conselho Nacional de Desenvolvimento Científico e Tecnológico (CNPq), Financiadora de Estudos e Projetos (FINEP): (01.13.0343.02), Fundação de Amparo a Pesquisa do Estado de Minas Gerais (FAPEMIG) and Rede Mineira de Química for the financial support.

References

1. Jain J, Arora S, Rajwade JM et al (2009) Silver nanoparticles in therapeutics: development of an antimicrobial gel formulation for topical use. Mol Pharm 6:1388–1401. https://doi.org/10.1021/mp900056g
2. Kalishwaralal K, BarathManiKanth S, Pandian SRK et al (2010) Silver nano—a trove for retinal therapies. J Control Release 145:76–90. https://doi.org/10.1016/J.JCONREL.2010.03.022
3. Byod A, Natuurkunde T, Hogeschool T, Delft CJ (1982) The polymorphism of silver tungstate Ag_2WO_4. J Appl Crystallogr 820:10114–10116
4. Haro Chávez NL, de Avila ED, Barbugli PA et al (2018) Promising effects of silver tungstate microcrystals on fibroblast human cells and three dimensional collagen matrix models: a novel non-cytotoxic material to fight oral disease. Colloids Surfaces B Biointerfaces 170:505–513. https://doi.org/10.1016/j.colsurfb.2018.06.023
5. Pereira PFS, Santos CC, Gouveia AF et al (2017) α-$Ag_{2-2x}Zn_xWO_4$ ($0 \le x \le 0.25$) solid solutions: structure, morphology, and optical properties. Inorg Chem 56:7360–7372. https://doi.org/10.1021/acs.inorgchem.7b00201
6. Lin Z, Li J, Zheng Z et al (2015) Electronic reconstruction of α-Ag_2WO_4 nanorods for visible-light photocatalysis. ACS Nano 9:7256–7265. https://doi.org/10.1021/acsnano.5b02077
7. Cavalcante LS, Almeida MAP, Avansi W et al (2012) Cluster coordination and photoluminescence properties of alpha-Ag_2WO_4 microcrystals. Inorg Chem 51:10675–10687
8. De Santana YVB, Gomes JEC, Matos L et al (2014) Silver molybdate and silver tungstate nanocomposites with enhanced photoluminescence. Nanomater Nanotechnol 4:22. https://doi.org/10.5772/58923
9. Pinatti IM, Nogueira IC, Pereira WS et al (2015) Structural and photoluminescence properties of Eu^{3+} doped α-Ag_2WO_4 synthesized by the green coprecipitation methodology. Dalton Trans 44:17673–17685. https://doi.org/10.1039/C5DT01997D
10. Zhang R, Cui H, Yang X et al (2012) Facile hydrothermal synthesis and photocatalytic activity of rod-like nanosized silver tungstate. Micro Nano Lett 7:1285–1288. https://doi.org/10.1049/mnl.2012.0765
11. Chen H, Xu Y (2014) Photoactivity and stability of Ag_2WO_4 for organic degradation inaqueous suspensions. Appl Surf Sci 319:319–323. https://doi.org/10.1016/j.apsusc.2014.05.115
12. Cabral AC, Cavalcante LS, Deus RC et al (2014) Photoluminescence properties of praseodymium doped cerium oxide nanocrystals. Ceram Int 40:4445–4453. https://doi.org/10.1016/j.ceramint.2013.08.117
13. Longo E, Volanti DP, Longo VM et al (2014) Toward an understanding of the growth of Ag filaments on α-Ag_2WO_4 and their photoluminescent properties: a combined experimental and theoretical study. J Phys Chem C 118:1229–1239. https://doi.org/10.1021/jp408167v
14. Aguir K, Mastelaro VR, Longo E (2014) A novel ozone gas sensor based on one-dimensional (1D) α-Ag_2WO_4 nanostructures. Nanoscale. https://doi.org/10.1039/c3nr05837a
15. Da Silva LF, Longo E, Catto AC et al (2016) Acetone gas sensor based on α-Ag_2WO_4 nanorods obtained via a microwave-assisted hydrothermal route. J Alloys Compd 683:186–190. https://doi.org/10.1016/j.jallcom.2016.05.078
16. Longo VM, De Foggi CC, Ferrer MM et al (2014) Potentiated electron transference in α-Ag_2WO_4 microcrystals with Ag nanofilaments as microbial agent. J Phys Chem A 118:5769–5778. https://doi.org/10.1021/jp410564p
17. Foggi CC, Fabbro MT, Santos LPS et al (2017) Synthesis and evaluation of A-Ag_2WO_4 as novel antifungal agent. Chem Phys Lett 674:125–129. https://doi.org/10.1016/j.cplett.2017.02.067
18. Roca RA, Sczancoski JC, Nogueira IC et al (2015) Facet-dependent photocatalytic and antibacterial properties of α-Ag_2WO_4 crystals: combining experimental data and theoretical insights. Catal Sci Technol 5:4091–4107. https://doi.org/10.1039/C5CY00331H
19. Selvamani M, Krishnamoorthy G, Ramadoss M et al (2016) Ag@Ag8W4O16nanoroasted rice beads with photocatalytic,

antibacterial and anticancer activity. Mater Sci Eng, C 60:109–118. https://doi.org/10.1016/j.msec.2015.11.002
20. Santos CJ, Ferreira Soares DC, de Ferreira CdeA et al (2018) Antiangiogenic evaluation of $ZnWO_4$ nanoparticles synthesised through microwave-assisted hydrothermal method. J Drug Target. https://doi.org/10.1080/1061186X.2018.1428810
21. Maier-Hauff K, Ulrich F, Nestler D et al (2011) Efficacy and safety of intratumoral thermotherapy using magnetic iron-oxide nanoparticles combined with external beam radiotherapy on patients with recurrent glioblastoma multiforme. J Neurooncol 103:317–324. https://doi.org/10.1007/s11060-010-0389-0
22. Beik J, Abed Z, Ghoreishi FS et al (2016) Nanotechnology in hyperthermia cancer therapy: from fundamental principles to advanced applications. J Control Release 235:205–221. https://doi.org/10.1016/j.jconrel.2016.05.062
23. Ingham B, Toney MF (2014) X-ray diffraction for characterizing metallic films. Met Film Electron Opt Magn Appl. https://doi.org/10.1533/9780857096296.1.3
24. Monteiro LOF, Fernandes RS, Oda CMR et al (2018) Biomedicine & Pharmacotherapy Paclitaxel-loaded folate-coated long circulating and pH-sensitive liposomes as a potential drug delivery system : a biodistribution study. Biomed Pharmacother 97:489–495. https://doi.org/10.1016/j.biopha.2017.10.135
25. Oda CMR, Fernandes RS, de Araújo Lopes SC et al (2017) Synthesis, characterization and radiolabeling of polymeric nanomicelles as a platform for tumor delivering. Biomed Pharmacother 89:268–275. https://doi.org/10.1016/j.biopha.2017.01.144
26. Soares DCF, Cardoso VN, de Barros ALB et al (2012) Antitumoral activity and toxicity of PEG-coated and PEG-folate-coated pH-sensitive liposomes containing (159)Gd-DTPA-BMA in Ehrlich tumor bearing mice. Eur J Pharm Sci 45:58–64. https://doi.org/10.1016/j.ejps.2011.10.018
27. Bilecka I, Niederberger M (2010) Microwave chemistry for inorganic nanomaterials synthesis. Nanoscale 2:1358. https://doi.org/10.1039/b9nr00377k
28. Perreux L, Loupy A (2001) A tentative rationalization of microwave effects in organic synthesis according to the reaction medium, and mechanistic considerations. Tetrahedron 57:9199–9223. https://doi.org/10.1016/S0040-4020(01)00905-X
29. Gedye R, Smith F, Westaway K et al (1986) The use of microwave ovens for rapid organic synthesis. Tetrahedron Lett 27:279–282. https://doi.org/10.1016/S0040-4039(00)83996-9
30. Giguere RJ, Bray TL, Duncan SM, Majetich G (1986) Application of commercial microwave ovens to organic synthesis. Tetrahedron Lett 27:4945–4948. https://doi.org/10.1016/S0040-4039(00)85103-5
31. Righettoni M, Tricoli A, Pratsinis SE (2010) Si:WO_3 sensors for highly selective detection of acetone for easy diagnosis of diabetes by breath analysis. Anal Chem 82:3581–3587. https://doi.org/10.1021/ac902695n
32. Kim DH, Shim YS, Jeon JM et al (2014) Vertically ordered hematite nanotube array as an ultrasensitive and rapid response acetone sensor. ACS Appl Mater Interfaces 6:14779–14784. https://doi.org/10.1021/am504156w
33. Muthamizh S, Giribabu K, Manigandan R, Praveen Kumar S, Munusamy S, Suresh R, Narayanan V (2016) Ag@Ag8W4O16 nanoroasted rice beads with photocatalytic, antibacterial and anticancer activity. Mater Sci Eng C 60(1):109–118
34. Pinatti IM, Fern GR, Longo E et al (2019) Luminescence properties of α-Ag_2WO_4 nanorods co-doped with Li + and Eu3 + cations and their effects on its structure. J Lumin 206:442–454. https://doi.org/10.1016/j.jlumin.2018.10.104
35. He H, Xue S, Wu Z et al (2016) Synthesis and characterization of robust Ag_2S/Ag_2WO_4 composite microrods with enhanced photocatalytic performance. J Mater Res 31:2598–2607. https://doi.org/10.1557/jmr.2016.284
36. Turkovič A, Fox DL, Scott JF et al (1977) High temperature Raman spectroscopy of silver tetratungstate, Ag8W4O16. Mater Res Bull 12:189–195. https://doi.org/10.1016/0025-5408(77)90163-5
37. Basiev T, Sobol A, Voronko Y, Zverev P (2000) Spontaneous Raman spectroscopy of tungstate and molybdate crystals for Raman lasers. Opt Mater (Amst) 15:205–216. https://doi.org/10.1016/S0925-3467(00)00037-9
38. Ernsting MJ, Murakami M, Roy A, Li S-DD (2013) Factors controlling the pharmacokinetics, biodistribution and intratumoral penetration of nanoparticles. J Control Release 172:782–794. https://doi.org/10.1016/j.jconrel.2013.09.013
39. Raza K, Kumar P, Kumar N, Malik R (2017) Pharmacokinetics and biodistribution of the nanoparticles. Adv Nanomedicine Deliv Ther Nucleic Acids. https://doi.org/10.1016/B978-0-08-100557-6.00009-2
40. De Barros ALB, De Oliveira Ferraz KS, Dantas TCS et al (2015) Synthesis, characterization, and biodistribution studies of ^{99m}Tc-labeled SBA-16 mesoporous silica nanoparticles. Mater Sci Eng, C 56:181–188. https://doi.org/10.1016/j.msec.2015.06.030
41. Psimadas D, Bouziotis P, Georgoulias P et al (2013) Radiolabeling approaches of nanoparticles with 99mTc. Contrast Media Mol Imaging 8:333–339. https://doi.org/10.1002/cmmi.1530
42. Snehalatha M, Venugopal K, Saha RN et al (2008) Etoposide loaded PLGA and PCL nanoparticles II: biodistribution and pharmacokinetics after radiolabeling with Tc-99m. Drug Deliv 15:277–287. https://doi.org/10.1080/10717540802006500
43. Psimadas D, Baldi G, Ravagli C et al (2012) Preliminary evaluation of a 99mTc labeled hybrid nanoparticle bearing a cobalt ferrite core: in vivo biodistribution. J Biomed Nanotechnol 8:575–585
44. Fu CM, Wang YF, Chao YC et al (2004) Directly labeling ferrite nanoparticles with Tc-99m radioisotope for diagnostic applications. IEEE Trans Magn 40:3003–3005. https://doi.org/10.1109/TMAG.2004.834199
45. Wang AY, Kuo CL, Lin JL et al (2010) Study of magnetic ferrite nanoparticles labeled with 99mTc-pertechnetate. J Radioanal Nucl Chem 284:405–413. https://doi.org/10.1007/s10967-010-0488-6
46. Meng Y, Zhang X-H, Du B-Y et al (2011) Thermosets with core–shell nanodomain by incorporation of core crosslinked star polymer into epoxy resin. Polymer (Guildf) 52:391–399. https://doi.org/10.1016/J.POLYMER.2010.11.046
47. Matsumura Y, Maeda H (1986) A new concept for macromolecular therapeutics in cnacer chemotherapy: mechanism of tumoritropic accumulatio of proteins and the antitumor agents Smancs. Cancer Res 46:6387–6392. https://doi.org/10.1021/bc100070g
48. Heneweer C, Holland JP, Divilov V et al (2011) Magnitude of enhanced permeability and retention effect in tumors with different phenotypes: 89Zr-albumin as a model system. J Nucl Med 52:625. https://doi.org/10.2967/JNUMED.110.083998